Evolution and function of the hominin forefoot

Peter J. Fernández[a,b,1], Carrie S. Mongle[c], Louise Leakey[d,e], Daniel J. Proctor[f], Caley M. Orr[g,h], Biren A. Patel[i,j], Sergio Almécija[k,l,m], Matthew W. Tocheri[n,o], and William L. Jungers[a,p]

[a]Department of Anatomical Sciences, Stony Brook University, Stony Brook, NY 11794; [b]Department of Biomedical Sciences, Marquette University, Milwaukee, WI 53202; [c]Interdepartmental Doctoral Program in Anthropological Sciences, Stony Brook University, Stony Brook, NY 11794; [d]Department of Anthropology, Stony Brook University, Stony Brook, NY 11794; [e]Turkana Basin Institute, Stony Brook University, Stony Brook, NY 11794; [f]Department of Anthropology, Lawrence University, Appleton, WI 54911; [g]Department of Cell and Developmental Biology, University of Colorado School of Medicine, Aurora, CO 80045; [h]Department of Anthropology, University of Colorado Denver, Denver, CO 80204; [i]Department of Integrative Anatomical Sciences, Keck School of Medicine, University of Southern California, Los Angeles, CA 90033; [j]Human and Evolutionary Biology Section, Department of Biological Sciences, University of Southern California, Los Angeles, CA 90089; [k]Division of Anthropology, American Museum of Natural History, New York, NY 10024; [l]Center for the Advanced Study of Human Paleobiology, Department of Anthropology, The George Washington University, Washington, DC 20052; [m]Institut Català de Paleontologia Miquel Crusafont (ICP), Universitat Autònoma de Barcelona, 08193 Cerdanyola del Vallès, Barcelona, Spain; [n]Department of Anthropology, Lakehead University, Thunder Bay, ON P7B 5E1, Canada; [o]Human Origins Program, National Museum of Natural History, Smithsonian Institution, Washington, DC 20013; and [p]Association Vahatra, Antananarivo 101, Madagascar

Edited by Bruce Latimer, Case Western Reserve University, Cleveland, OH, and accepted by Editorial Board Member C. O. Lovejoy July 12, 2018 (received for review January 15, 2018)

The primate foot functions as a grasping organ. As such, its bones, soft tissues, and joints evolved to maximize power and stability in a variety of grasping configurations. Humans are the obvious exception to this primate pattern, with feet that evolved to support the unique biomechanical demands of bipedal locomotion. Of key functional importance to bipedalism is the morphology of the joints at the forefoot, known as the metatarsophalangeal joints (MTPJs), but a comprehensive analysis of hominin MTPJ morphology is currently lacking. Here we present the results of a multivariate shape and Bayesian phylogenetic comparative analyses of metatarsals (MTs) from a broad selection of anthropoid primates (including fossil apes and stem catarrhines) and most of the early hominin pedal fossil record, including the oldest hominin for which good pedal remains exist, *Ardipithecus ramidus*. Results corroborate the importance of specific bony morphologies such as dorsal MT head expansion and "doming" to the evolution of terrestrial bipedalism in hominins. Further, our evolutionary models reveal that the MT1 of *Ar. ramidus* shifts away from the reconstructed optimum of our last common ancestor with apes, but not necessarily in the direction of modern humans. However, the lateral rays of *Ar. ramidus* are transformed in a more human-like direction, suggesting that they were the digits first recruited by hominins into the primary role of terrestrial propulsion. This pattern of evolutionary change is seen consistently throughout the evolution of the foot, highlighting the mosaic nature of pedal evolution and the emergence of a derived, modern hallux relatively late in human evolution.

bipedalism | hominin evolution | metatarsals | *Ardipithecus* | functional morphology

The obligate terrestrial bipedalism of modern humans is unique among extant primates, and its ancient adoption by early hominins impacted subsequent evolutionary changes in social behavior and the development of material culture. A suite of morphological changes in the feet of early hominins is associated with the evolution of habitual bipedal locomotion in the human career and ultimately led to the energetically efficient gait used by modern humans (1–5).

The forefoot skeleton includes the metatarsals (MT) and phalanges, and its functional anatomy is strongly tied to the evolution of bipedalism in hominins (5–9). Thus, hominin forefoot fossils can offer key insights into when and how bipedalism evolved in the human lineage. During bipedal walking, modern humans dorsiflex (i.e., hyperextend) their forefoot joints, specifically at the metatarsophalangeal joints (MTPJs), as part of the push-off phase of gait, which tightens plantar soft tissues to convert the foot into a relatively stiff, propulsive lever (10) (also see ref. 11). Features of MT head morphology such as "dorsal doming" are thought to facilitate this stiffening mechanism (6, 12); doming occurs when the distal articular surface expands and becomes particularly pronounced dorsally. Comparative analysis of humans and chimpanzees has shown that dorsal doming is correlated with in vivo ranges of motion at the MTPJs, with humans displaying greater doming and a greater range of MTPJ dorsiflexion during bipedalism (9).

The form and function of the hominin forefoot have been studied extensively (5, 6, 13–16), especially in light of more recent discoveries of hominin pedal fossils (17–19). However, a quantitative analysis of the hominin forefoot in a broad phylogenetic context is lacking, despite the theorized importance of these bony elements to the biomechanical demands of bipedalism (10, 20). To better understand the adaptive evolution of bipedalism in early hominins we investigated MTPJ morphology in Plio-Pleistocene fossil hominins (including species of *Ardipithecus*, *Australopithecus*, *Paranthropus*, and *Homo*) and a comparative sample of fossil and extant anthropoids (including modern humans, apes, and monkeys) using shape analyses and phylogenetic comparative methods to test hypotheses about the nature and timing of forefoot evolution in the human clade. Three-dimensional geometric morphometric techniques were used to quantify MT1–MT5 head shapes, and a multioptima Ornstein-Uhlenbeck (OU) model was used to estimate the placement and

Significance

A critical step in the evolutionary history leading to the origins of humankind was the adoption of habitual bipedal locomotion by our hominin ancestors. We have identified novel bony shape variables in the forefoot across extant anthropoids and extinct hominins that are linked functionally to the emergence of bipedal walking. Results indicate a consistent and generalizable pattern in hominin pedal evolution that spans from *Ardipithecus* to early *Homo*—the relatively late derivation of a modern hallux in comparison with the lateral rays. These data provide novel morphological and macroevolutionary evidence for how and when the hominin pedal skeleton evolved to accommodate the unique biomechanical demands of bipedalism.

Author contributions: P.J.F., S.A., and W.L.J. designed research; P.J.F. and C.S.M. performed research; P.J.F., C.S.M., L.L., D.J.P., C.M.O., B.A.P., S.A., M.W.T., and W.L.J. contributed new reagents/analytic tools; P.J.F. and C.S.M. analyzed data; and P.J.F., C.S.M., and W.L.J. wrote the paper with input from all authors.

The authors declare no conflict of interest.

This article is a PNAS Direct Submission. B.L. is a guest editor invited by the Editorial Board.

Data deposition: The raw data are available through Open Science Framework (https://osf.io/4fc7b/).

[1]To whom correspondence should be addressed. Email: pedro.fernandez@marquette.edu.

This article contains supporting information online at www.pnas.org/lookup/suppl/doi:10.1073/pnas.1800818115/-/DCSupplemental.

Published online August 13, 2018.

magnitude of adaptive shifts in the evolution of MTPJ morphology for each toe (21). To better calibrate the ancestral state estimation of the chimpanzee-human and other last common ancestors (LCAs), stem catarrhines (e.g., *Catopothecus*, *Epipliopithecus*) and Miocene apes (e.g., *Ekembo* sp.) were also included in the analysis. Although the distal half of the MTPJ joint, the proximal phalangeal base, also plays an important role in the articular mechanics of the hominin forefoot (6, 7), a comprehensive analysis of its articular surface is outside the scope of this study. Moreover, hominin forefoot fossils are typically found in isolation, and thus it is informative to discern to what extent locomotor behavior in these extinct groups can be determined from single, isolated elements. Finally, there is evidence that 3D analysis of the distal MT articular surface is more functionally informative than the proximal phalangeal base, which seems to track phylogeny more closely than function (22).

Results

Across the entire forefoot (MT1–MT5), shape variables principal component 1 (PC1) and principal component 2 (PC2) (explaining 23–29% and 12–16% of total variance, respectively) track MT head orientation and robusticity in a pattern similar to that found by previous research (ref. 8 and Fig. 1). Because the fifth MTPJ (MTPJ5) plays a relatively reduced role in bipedal forefoot mechanics (9), results for MT5 are not reported in further detail. PC1 primarily explains variance in MT head shape that is related to expanded articular surfaces (i.e., robusticity). For MT1, as an example, high PC1 scores reflect dorsally wider hallucal heads and broader plantar surfaces with shallow grooves for the sesamoids, a pattern particularly pronounced in the modern human sample. Shape warps constructed in 3D using low PC1 scores display marked plantar wedging of the MT head, with strongly angled facets/grooves for the hallucal sesamoids—morphology typical of extant great apes. PC2 captures variance in the overall dorsal vs. plantar orientation of the MT head, as well as the degree to which the head projects above the diaphysis (i.e., dorsal doming or bulging). For 3D warps with high PC2 scores, the resulting shapes have a dorsally oriented MT head, but the dorsal part of the head is rounded and narrow, a mosaic pattern seen in some fossil

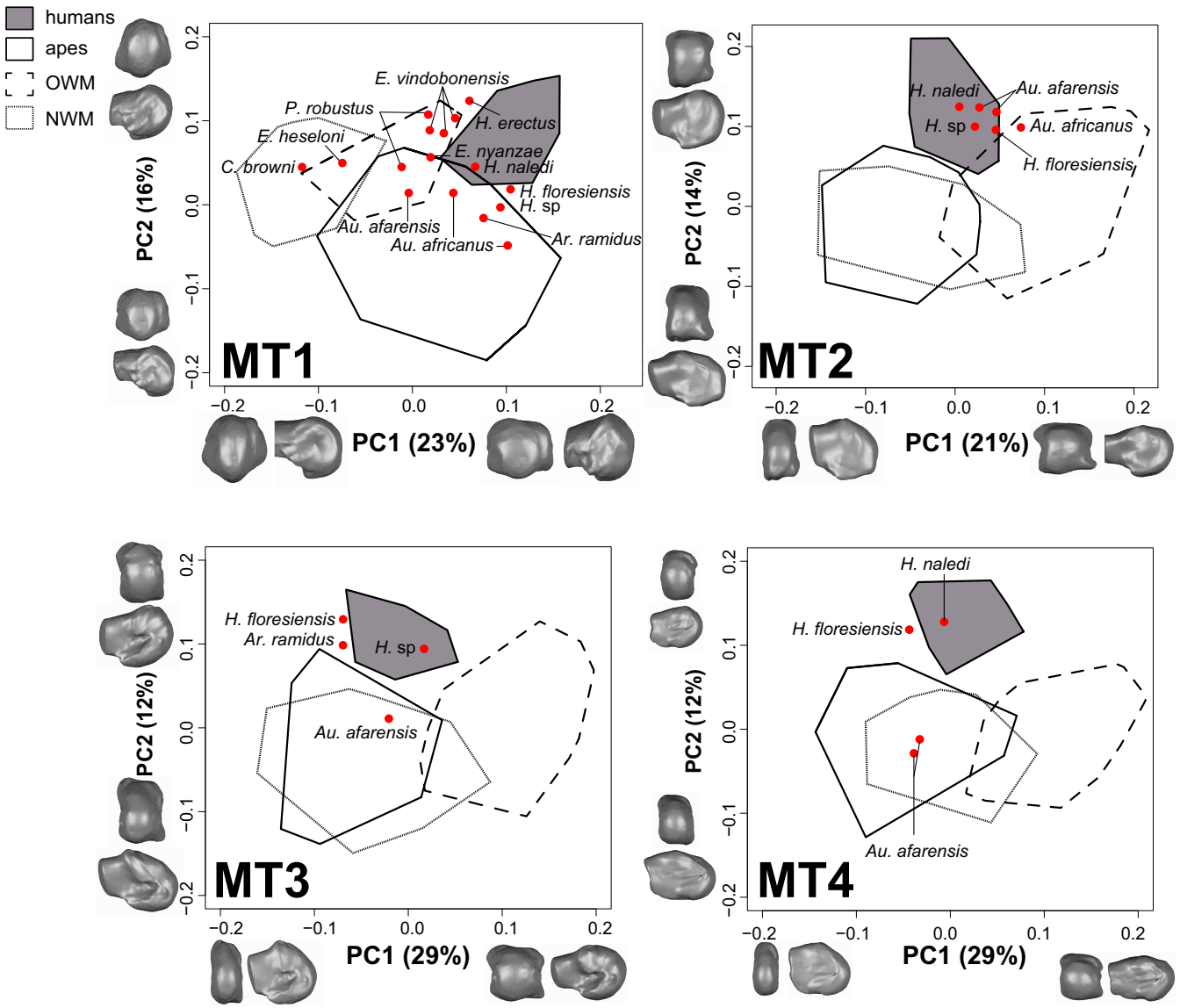

Fig. 1. PCA scatterplots of PC1 vs. PC2 for MT1–MT4 morphospaces. MT1, most hominins are more ape-like in morphology (except *H. naledi*); MT2, most hominins are modern human-like; MT3, most hominins are modern human-like except *Au. afarensis*, but this may be due to taphonomy (see main text) (note that the *Ar. ramidus* MT3 appears more modern human-like than does its corresponding MT1); MT4, the results are similar to MT3. *C. browni, Catopithecus browni; E. vindobonensis, Epipliopithecus vindobonensis*; PCA, principal component analysis.

hominins. Low PC2 scores describe a plantarly oriented MT head, which is best observed in great apes.

Results from the multioptima OU models show different patterns in evolutionary adaptive shifts depending on the shape variable studied. The results from the bayou models of MT1–MT5 PC1 are largely similar, with minor differences in the adaptive optima among platyrrhines. In PC2, which captures MT head morphology related specifically to dorsal doming, adaptive shifts are typically found at the base of the hominin lineage (Fig. 2) or solely within the genus *Homo*. This finding provides evidence that morphological variation captured in PC2 is related to the advent of bipedalism in early hominin groups. Because PC1 is most biased by traits varying early in the tree (23) and PC2 appears to capture functionally relevant morphological changes unique to hominins, we emphasize results from the bayou models of this latter shape variable in more detail below.

Fossil hominin and catarrhine MT1 head morphology is variable, spanning much of anthropoid morphospace (Fig. 1). The stem catarrhines all fall within the Old World and New World monkey (OWM and NWM, respectively) minimum convex polygons. The Miocene ape specimens were more intermediate between monkey and extant ape morphology. This is especially true for *Ekembo nyanzae* (KNM-RU 17392), whose morphology overlapped the OWM and ape distributions in the morphospace. *Ekembo heseloni* (KNM-KPS III) was more monkey-like, falling in a region of OWM and NWM overlap. The geologically oldest hominin MT1 studied here is the ∼4.4-Ma-old *Ardipithecus ramidus* (ARA-VP-6/500-089), which falls within the extant ape distribution of the morphospace. In particular, the *Ar. ramidus* hallux appears most similar to that of gorillas based on the results of this analysis. Similar results characterize the MT1s of *Australopithecus afarensis* (A.L. 333-115A; ∼3.2 Ma) and *Australopithecus africanus* (StW 595 and StW 562; ∼2.0–2.6 Ma), both of which fall outside the modern human range of variation. Some caution is warranted for StW 595 because this specimen displays some damage to the dorsal surface of the MT head, making it difficult to ascertain where its original articular surface terminated. *Paranthropus robustus* (SK 1813 and SKX 5017; ∼1.1–1.8 Ma) overlaps with modern humans on PC2, but their mediolaterally gracile MT1s more closely resemble those of apes and OWMs, as reflected by their scores along PC1. An early *Homo* MT1 (KNM-ER 64062; ∼1.8 Ma) exhibits a very human-like dorsal head orientation, but its relatively narrow, rounded head and plantar condylar morphology pushes it outside the range of modern humans. *Homo floresiensis* (LB1/21; ∼0.08 Ma) displays a similar MT1 morphology to early *Homo* and falls just outside the range of modern human variation. Finally, the MT1 of *Homo naledi* (UW 101-1443; ∼0.2–0.3 Ma) is the only fossil in our study to fall directly within the modern human distribution, whereas most other fossils overlap with modern humans only on PC1. Both early *Homo* and *H. naledi* are within the modern human morphospace when the comparative sample excludes monkeys. The bayou model identifies two shifts (posterior probability > 0.25) in the posterior distribution of the MT1 PC2 analysis. Shifts related to more dorsal head orientation are detected at the base of the hominin clade, as well as at the transition from the earliest hominin in the sample (*Ar. ramidus*) to later australopiths. This finding supports previous observations of the *Ardipithecus* forefoot morphology (24–26).

Unlike the MT1, the lateral MTs of fossil hominins are more like modern humans. For MT2 (Fig. 1), *Au. afarensis* (A.L. 333-115B, A.L. 333-72), early *Homo* (KNM-ER 64062), *H. floresiensis*

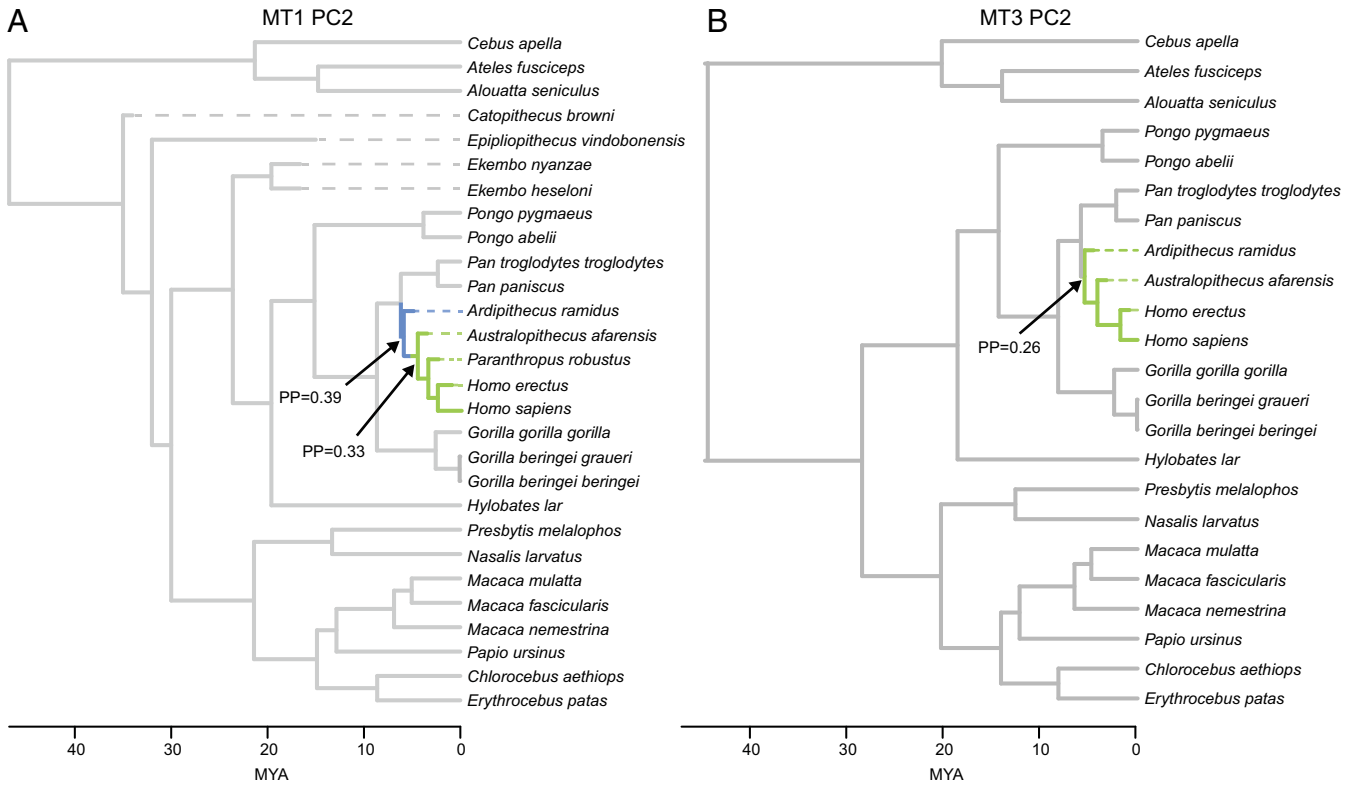

Fig. 2. Time-scaled phylogenetic tree showing estimated adaptive regimes from the multioptima OU model. Adaptive optima are estimated for the PC2 scores of the MT1 (*A*) and MT3 (*B*). Adaptive shifts are indicated with an arrow when the posterior probabilities of a shift at a given node was >0.25. Branches are colored according to different adaptive regimes. Note that two adaptive shifts occur in the MT1 PC2 shape data compared with only one shift in the MT2–MT5 shape data. This finding suggests that the hallux underwent significant shape changes during human evolution even after facultative bipeds (e.g., *Ar. ramidus*) had evolved (24–26), more so than what was seen in the lateral MTs, which had evolved derived modern human-like shapes relatively early in the fossil record (also see ref. 53). (Scale bar in Ma.) PP, posterior probability.

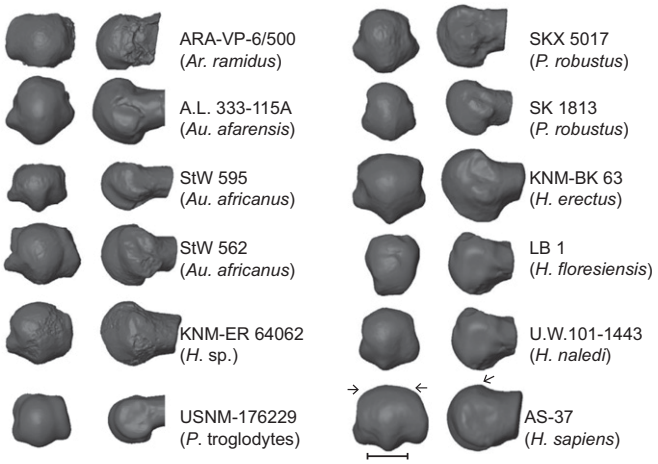

Fig. 3. Distal (*Left*) and lateral (*Right*) views of fossil hominin and modern human first MT (MT1) heads. Note that *H. sapiens* is characterized by dorsal overlap of the distal articular surface onto the MT shaft and by wide flattening of the dorsal articular surface (arrows). (Scale bar: 1 cm.) *H. erectus*, *Homo erectus*; *P. troglodytes*, *Pan troglodytes*.

(LB1/22), and *H. naledi* (U.W. 101–1458) all fall within the modern human convex polygon. Early *Homo* and *Au. afarensis* fall toward the extreme perimeter of the modern human distribution due to high PC1 scores, whereas the other hominin fossils fall close to the mean value for modern humans. StW 89, a putative *Au. africanus* MT2 (16), has a PC1 score that is outside the range of modern human variation. Only one well-supported shift is identified by the bayou model of MT2 PC2 scores. Importantly, this shift toward a dorsally domed morphology is detected at the transition between *Au. africanus* and later members of the genus *Homo*. However, we note that the unusual morphology observed in StW 89 could be biasing the inferred placement of this shift, especially given that *Au. afarensis* appears more human-like in its morphology as captured along PC2.

In the MT3 dataset, *Ar. ramidus* (ARA-VP-6/500-505) plots closely to the modern human distribution, falling just outside due to a low PC1 score (Fig. 1). This is in sharp contrast to the *Ar. ramidus* MT1, which displays a more ape-like anatomy. The MT3 of *Au. afarensis* (A.L. 333-115C) falls within the ape distribution, unlike the MT2 from the same foot, which appears modern human-like. However, this result may be influenced by taphonomic damage to the dorsal aspect of this particular MT3 (9, 13). Early *Homo* (KNM-ER 64062) and *H. floresiensis* (LB1/23) fall within and just outside the range of modern human variation, respectively. The bayou model identifies one well-supported shift at the base of the hominin clade in the posterior distribution of the MT3 PC2 analysis (Fig. 2*B*). This shift toward increased dorsal doming/bulging indicates that adaptations for bipedalism occurred early in the lateral forefoot of hominins, at least by 4.4 Ma.

For the MT4, *Au. afarensis* (A.L. 333-115D and A.L. 333-160) head shape plots most closely to that of apes, whereas later hominins (*H. floresiensis*, *H. naledi*) fall closer to the modern human shape distribution (Fig. 1). A well-preserved, intact MT4 of *Au. afarensis* (A.L. 333-160) has been argued to display modern human-like morphology (15); however, results from our shape analysis indicate a more ape-like distal morphology. *H. floresiensis* (LB1/24) falls well within the modern human range along PC2 but retains an ape-like PC1 score, and thus occupies an intermediate portion of the morphospace between apes and humans. The complete *H. naledi* MT4 (U.W. 101-269) again falls within the modern human range of variation. One shift (>0.25), restricted to dorsal doming in modern humans, is detected in the posterior distribution of the MT4 PC2 bayou analysis.

Discussion

Fossil hominins exhibit a remarkable mosaicism in their forefoot joint anatomy. This is especially true for the hallux (MT1), where all hominins except for *H. naledi* fall outside the ranges of modern human variation for variables related to MT1 head orientation and dorsal doming. Although the hallux of most fossil hominins is domed like that of modern humans [except for *Ardipithecus* (25)], many of them lack mediolaterally flattened and expanded dorsal articular surfaces, which presumably helps stabilize the joint in modern humans during peak loading at the end of the single support phase of the gait cycle (5, 12). This finding, especially evident in *P. robustus* and *Au. afarensis*, provides further evidence that these hominins lacked the full suite of derived pedal characteristics seen in modern humans. This implies that pedal biomechanics in these fossil hominins may be related to a more mixed, versatile locomotor repertoire (27, 28) and/or to more lateral aspects of the foot being involved in toe-off (29). Emphasis on the lateral part of the forefoot in the propulsive phase of bipedalism is evident in the foot of *Ardipithecus* and presumably represents the primitive condition for bipedal hominins (25, 27).

For MT2–MT5, fossil hominins often fall within the modern human range of shape variation on both PC1 and PC2. This is especially true for MT2, with only StW 89 falling just outside the modern human range of variation on both PCs. StW 89 is typically attributed to *Au. africanus*, but this attribution is not definitive as there are no associated craniodental remains. Interestingly, StW 89 was intermediate between cercopithecoids and modern humans in a study of MT torsion (30). However, StW 89 does not particularly resemble a cercopithecoid MT in overall form either (i.e., it lacks a curved diaphysis and mediolaterally broad proximal articular surface). If it belongs to *Au. africanus*, then this hominin is similar to *Au. afarensis* (and modern humans) on PC2 and is thus certainly dorsally "domed," but its morphology on PC1 remains unique among hominins. Future MT head fossil discoveries from South Africa, particularly those of *Australopithecus sediba*, might help clarify the taxonomic attribution StW 89. Shape analysis of the *Au. afarensis* forefoot has been discussed elsewhere (9) but, in brief, this hominin shows a mix of modern human-like and ape-like MTs across its lateral forefoot.

Results from the multioptima OU analysis clearly illustrate the importance of PC2 shape changes (e.g., dorsal MT head orientation and doming) to the evolution of terrestrial bipedalism in hominins, while PC1 appears to capture an overall phylogenetic signal (i.e., it separates major anthropoid clades) and is not specific to bipeds. In accordance with White et al. (24), our analyses recovered that the MT1 of *Ar. ramidus* shifts away from the reconstructed optimum of our LCA with apes but not necessarily in the direction of modern humans. The *Ar. ramidus* morphotype displays a unique adaptive suite of MT1 morphology captured by PC2, reflective of incipient adaptation to terrestrial bipedalism with retained primitive opposability. The adaptive shift away from the LCA (and *Homo*) MT1 morphotype suggests that *Ardipithecus* captures the beginning of an adaptive radiation in hallucal MTPJ morphology in response to the advent of bipedalism in the hominin lineage. Although *Ardipithecus* was facultatively bipedal on the ground, aspects of its MT1 and much of its postcranial skeleton generally suggest it likely spent a significant amount of time in the trees. That said, our data are largely compatible with arboterrestrial "multigrady" (24) but provide no evidence for above-branch adaptations to quadrupedal plantigrady in this species, at least insofar as its forefoot functional morphology is concerned. Moreover, grounding this model of pedal transformation by inclusion of Miocene fossils such as *Ekembo* improves our ability to infer evolutionary trends through time.

In contrast to its MT1, the lateral rays of *Ardipithecus* shift in a direction that would suggest that they "took on the primary role of terrestrial propulsion" (ref. 24, p. 4879); this evolutionary change precedes a modern human-like morphology in the hallux and is consistently seen throughout human evolution. The lateral

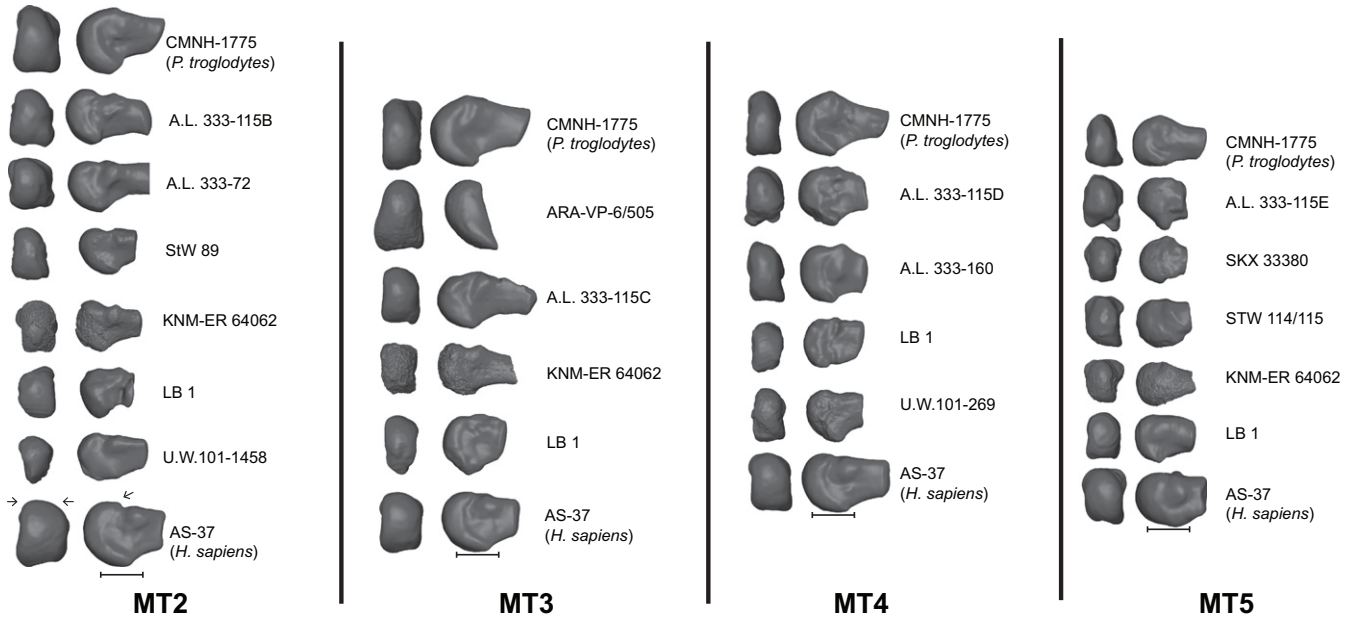

Fig. 4. Distal (*Left*) and lateral (*Right*) views of fossil hominin and modern human lateral MT (MT2–MT5) heads. Note that *Homo sapiens* is characterized by dorsal overlap of the distal articular surface onto the MT shaft and by wide flattening of the dorsal articular surface. Note epicondylar surface landmarks were removed for MT3 analyses to include *Ar. ramidus* (ARA-VP-6/505) into the analysis. (Scale bar: 1 cm.) *P. troglodytes*, *Pan troglodytes.*

rays take on the primary role of terrestrial propulsion in early hominins like *Ardipithecus* because the hallux is arranged for powerful pedal grasping in these taxa, unlike the hallux of later hominins and modern humans, whose hallux is arranged for generating push-off power at the end of stance phase in the bipedal gait cycle. It was the lateral forefoot that first took up this functional role in hominins, while the hallux morphology suggests a retention of grasping capabilities or a less efficient push-off mechanism that lingered until relatively late in hominin evolution.

Materials and Methods

Extant and Fossil Sample. Shape differences in MT1–MT5 were quantified for extant comparative (n = 1,738; *SI Appendix*, Table S1) and fossil catarrhine (n = 35; Figs. 3 and 4 and *SI Appendix*, Table S2) samples. Male-to-female sex ratios were nearly even, although sex was unknown for the *Homo sapiens* sample. In highly dimorphic species (e.g., *Gorilla*, *Pongo*), statistical tests for sex differences were performed; no significant differences were found, and thus the data were pooled. The presumably unshod (31–33) populations collected at the Iziko Museum at Cape Town and the University of Cape Town come from prepastoral, Late Stone populations in South Africa, and the dated material ranged from 9000 to 2000 y B.P. Only adult, nonpathological specimens were sampled. The *Ardipithecus* fossils (ARA-VP-6/500-089, ARA-VP-6/500-505) were micro-computed tomography (μCT) scanned by Dr. Gen Suwa and Dr. Tim White at an 80-μm isotropic voxel resolution (25), and then 3D polygons were reconstructed from these μCT data for use in this analysis. The *Au. afarensis* material included (A.L. 333-115A–E, A.L. 333-72, A.L. 333-160) were scanned on high-resolution, research-quality casts without reconstruction located at the Institute of Human Origins (Arizona State University). Scans from the *H. naledi* material were obtained from Morphosource (18). Details of the MT1 fossils of *Catopithecus*, *Epipliopithecus*, and *Ekembo* can be found elsewhere (34, 35).

3D Data Collection Procedures. Distal metatarsal morphology was explored using 3D digital polygon models reconstructed from either CT or μCT, as well as from 3D laser surface scans (36, 37). Laser scanning was conducted using a NextEngine 3D laser scanner (10,000 points per square inch resolution per scan, 12 scans per bone).

Morphometric Analysis. The 3D shapes of all five MT heads were evaluated using a landmark-based approach. A 5 × 5 3D surface patch of nine user-defined landmarks and semilandmarks was applied using Landmark Editor (38) following the methods detailed in ref. 8 (*SI Appendix*, Fig. S1). This landmark set has been shown to be replicable while also capturing the full articular surface morphology of the MT head. The surface patch was bounded mediolaterally by the proximal termination of the distal epicondyles, dorsally at the proximal termination of the distal articular surface, and plantarly at the proximal termination of the plantar condyles. See *SI Appendix*, Table S3 for specific anatomical locations of each landmark.

Because MT1 differs from MT2–5 in its ontogenetic development and gene expression (39), it possesses a unique shape that presents possible homology problems with the surface landmarks used in MT2–5. Therefore, MT1 morphometric data were analyzed separately from those of the lesser toes. Semilandmarks were slid using the minimized Procrustes distance criterion (40), but similar results were obtained using minimized bending energy algorithms (41). The slid coordinates were then subjected to a generalized Procrustes analysis (42), and principal component analysis was used to summarize and explore the observed variation in MT head shape. Articular surface wireframes and polygonal mesh warps were constructed to visualize shape changes using Thin-Plate Splines deformation (43). Significant differences in PC scores between taxonomic groups were analyzed using multivariate ANOVA; Tukey's honestly significant difference (HSD) was used for pairwise post hoc between-species and between-ray comparisons. All PCs explaining ≥5% of the total shape variance were subjected to these analyses, but because the study sample completely overlapped in all PCs beyond the first two, only the results from PC1 and PC2 are presented. Semilandmark sliding, generalized Procrustes analysis, principal component analysis, and linear regression analyses were performed in the R package "geomorph" (version 2.17) (44, 45). All statistical tests and associated graphics were executed in the R 3.2.2 base package (https://www.R-project.org). Thin-Plate Splines deformation shape visualizations were performed in Landmark Editor and MorphoJ (version 1.06b) (46).

Phylogenetic OU Modeling. Phylogenetic comparative analyses were conducted using the primate molecular consensus tree from the 10K Trees Project (47). Hominin fossil taxa were introduced to the tree post hoc only when the phylogenetic placement of the taxa was relatively well resolved. The hominin phylogeny was added post hoc to the anthropoid molecular phylogeny based on Strait and Grine (48), with some nomenclatural differences and the addition of new hominin taxa. Similarly, other fossil primates (i.e., *Catopithecus*, *Epipliopithecus*, and *Ekembo*) were incorporated into the extant anthropoid phylogeny according to the relationships reconstructed by Stevens et al. (49).

To estimate the placement and magnitude of an adaptive shift in the evolution of MTPJ morphology, we applied a reversible-jump Bayesian

method to the PC1 and PC2 scores of each metatarsal. This multioptima OU method is an adaptation of the traditional OU model, which allows the model parameter theta (θ) to vary (21). This method is implemented in the R package "bayou" (21). Parameter priors suggested by Uyeda and Harmon (21) for continuous phenotypic trait data were used. The analysis was run for 1,000,000 generations with 20% burn-in removed. A second chain with independent starting positions was run, and convergence between the chains was determined by estimating Gelman's R statistic for each parameter (50). Adaptive shifts were considered well supported if their respective posterior probability exceeded 0.25 (23). Simulation studies have indicated that these modeling approaches are relatively robust to false-positive results (21, 51). Furthermore, results were subjected to a signal-to-noise ratio test following Cressler et al. (52) to assess effect size.

ACKNOWLEDGMENTS. We thank T. White, G. Suwa, and O. Lovejoy for access to the *Ardipithecus* fossil scans and helpful discussion. Surface models of *H. naledi* fossils were obtained from Morphosource, with thanks to L. Berger and colleagues. Access to additional fossil casts was made available by W. Kimbel, H. Dunsworth, and J. Fleagle. We are grateful to museum curatorial managers and staff for access to extant specimens in their care, including N. Duncan, E. Westwig, D. Lunde, N. Edmison, J. Dines, T. Kensler, L. Jellema, J. Chupasko, M. Omura, E. Gilissen, W. Seconna, and E. Bartnick. CT and μCT scans of some of the comparative sample were made possible with help from S. Judex, T. Skorka, and the staff in the Radiology Department at Stony Brook University. Last, we thank W. Wiedemann for assistance in data processing and N. Holowka for helpful discussion. Funding was provided by the Wenner-Gren Foundation; the Leakey Foundation; the Canada Research Chairs program; the Social Sciences and Humanities Research Council of Canada (Insight Grant 435-2017-1234); National Science Foundation Grants BCS-1539741, BCS-1317047, and BCS-1316947; the NIH (to the Caribbean Primate Research Center; Grant NIH 8 P40 OD012217-25); Spanish Ministerio de Economía y Competitividad Grant CGL2017-82654-P; the Generalitat de Catalunya (CERCA Program); and the W. Burghardt Turner Fellowship Program.

1. Morton DJ (1922) Evolution of the human foot. *Am J Phys Anthropol* 5:305–336.
2. Elftman H, Manter J (1935) Chimpanzee and human feet in bipedal walking. *Am J Phys Anthropol* 20:69–79.
3. Wood-Jones F (1944) *Structure and Function as Seen in the Foot* (Bailliere and Co., London).
4. Lewis OJ (1980) The joints of the evolving foot. Part III. The fossil evidence. *J Anat* 131: 275–298.
5. Susman RL (1983) Evolution of the human foot: Evidence from Plio-Pleistocene hominids. *Foot Ankle* 3:365–376.
6. Latimer B, Lovejoy CO (1990) Metatarsophalangeal joints of *Australopithecus afarensis*. *Am J Phys Anthropol* 83:13–23.
7. Griffin NL, D'Août K, Richmond B, Gordon A, Aerts P (2010) Comparative in vivo forefoot kinematics of *Homo sapiens* and *Pan paniscus*. *J Hum Evol* 59:608–619.
8. Fernández PJ, et al. (2015) Functional aspects of metatarsal head shape in humans, apes, and Old World monkeys. *J Hum Evol* 86:136–146.
9. Fernández PJ, Holowka NB, Demes B, Jungers WL (2016) Form and function of the human and chimpanzee forefoot: Implications for early hominin bipedalism. *Sci Rep* 6:30532.
10. Hicks JH (1954) The mechanics of the foot: II. The plantar aponeurosis and the arch. *J Anat* 88:25–30.
11. Holowka NB, O'Neill MC, Thompson NE, Demes B (2017) Chimpanzee and human midfoot motion during bipedal walking and the evolution of the longitudinal arch of the foot. *J Hum Evol* 104:23–31.
12. Susman RL, Brain TM (1988) New first metatarsal (SKX 5017) from Swartkrans and the gait of *Paranthropus robustus*. *Am J Phys Anthropol* 77:7–15.
13. Latimer BM, Lovejoy CO, Johanson DC, Coppens Y (1982) Hominid tarsal, metatarsal, and phalangeal bones recovered from the Hadar formation: 1974–1977 collections. *Am J Phys Anthropol* 57:701–719.
14. Jungers WL, et al. (2009) The foot of *Homo floresiensis*. *Nature* 459:81–84.
15. Ward CV, Kimbel WH, Johanson DC (2011) Complete fourth metatarsal and arches in the foot of *Australopithecus afarensis*. *Science* 331:750–753.
16. DeSilva JM, Proctor DJ, Zipfel B (2012) A complete second metatarsal (StW 89) from Sterkfontein member 4, South Africa. *J Hum Evol* 63:487–496.
17. Haile-Selassie Y, et al. (2012) A new hominin foot from Ethiopia shows multiple Pliocene bipedal adaptations. *Nature* 483:565–569.
18. Harcourt-Smith WEH, et al. (2015) The foot of *Homo naledi*. *Nat Commun* 6:8432.
19. Jungers WL, et al. (2015) New hominin fossils from Ileret (Kolom Odiet), Kenya. *Am J Phys Anthropol* 156:181.
20. Bojsen-Møller F (1979) Calcaneocuboid joint and stability of the longitudinal arch of the foot at high and low gear push off. *J Anat* 129:165–176.
21. Uyeda JC, Harmon LJ (2014) A novel Bayesian method for inferring and interpreting the dynamics of adaptive landscapes from phylogenetic comparative data. *Syst Biol* 63:902–918.
22. Fernández PJ (2016) Form and function of the anthropoid forefoot. PhD dissertation (Stony Brook University, Stony Brook, NY).
23. Uyeda JC, Caetano DS, Pennell MW (2015) Comparative analysis of principal components can be misleading. *Syst Biol* 64:677–689.
24. White TD, Lovejoy CO, Asfaw B, Carlson JP, Suwa G (2015) Neither chimpanzee nor human, *Ardipithecus* reveals the surprising ancestry of both. *Proc Natl Acad Sci USA* 112:4877–4884.
25. Lovejoy CO, Latimer B, Suwa G, Asfaw B, White TD (2009) Combining prehension and propulsion: The foot of *Ardipithecus ramidus*. *Science* 326:72e1–72e8.
26. Lovejoy CO, Suwa G, Simpson SW, Matternes JH, White TD (2009) The great divides: *Ardipithecus ramidus* reveals the postcrania of our last common ancestors with African apes. *Science* 326:100–106.
27. Stern JT, Jr, Susman RL (1983) The locomotor anatomy of *Australopithecus afarensis*. *Am J Phys Anthropol* 60:279–317.
28. Susman RL, Stern JT, Jr, Jungers WL (1984) Arboreality and bipedality in the Hadar hominids. *Folia Primatol (Basel)* 43:113–156.
29. Pontzer H, et al. (2010) Locomotor anatomy and biomechanics of the Dmanisi hominins. *J Hum Evol* 58:492–504.
30. Drapeau MSM, Harmon EH (2013) Metatarsal torsion in monkeys, apes, humans and australopiths. *J Hum Evol* 64:93–108.
31. Stock J, Pfeiffer S (2001) Linking structural variability in long bone diaphyses to habitual behaviors: Foragers from the southern African later stone age and the Andaman Islands. *Am J Phys Anthropol* 115:337–348.
32. Roberts N (1989) *The Holocene—An Environment History* (Basil Blackwell, Inc., Oxford).
33. Sealy J, Pfeiffer S (2000) Diet, body size, and landscape use among Holocene people in the Southern Cape, South Africa. *Curr Anthropol* 41:642–655.
34. Patel BA, et al. (2012) New primate first metatarsals from the Paleogene of Egypt and the origin of the anthropoid big toe. *J Hum Evol* 63:99–120.
35. Patel BA, Yapuncich GS, Tran C, Nengo IO (2017) Catarrhine hallucal metatarsals from the early Miocene site of Songhor, Kenya. *J Hum Evol* 108:176–198.
36. Tocheri MW, et al. (2011) Ecological divergence and medial cuneiform morphology in gorillas. *J Hum Evol* 60:171–184.
37. Shearer BM, et al. (2017) Evaluating causes of error in landmark-based data collection using scanners. *PLoS One* 12:e0187452.
38. Wiley DF, et al. (2005) Evolutionary morphing. *IEEE Visualization* 5:431–438.
39. Indjeian VB, et al. (2016) Evolving new skeletal traits by cis-regulatory changes in bone morphogenetic proteins. *Cell* 164:45–56.
40. Rohlf FJ (2010) tspRelw: Relative Warps Analysis, version 1.49 (Department of Ecology and Evolution, University of New York at Stony Brook, Stony Brook, NY).
41. Bookstein FL (1997) *Morphometric Tools for Landmark Data: Geometry and Biology* (Cambridge Univ Press, Cambridge, UK).
42. Gower JC (1975) Generalized procrustes analysis. *Psychometrika* 40:33–51.
43. Bookstein FL (1989) Principal warps: Thin-plate splines and the decomposition of deformations. *IEEE Comput Soc* 11:567–585.
44. Adams DC, Collyer ML, Otárola-Castillo E, Sherratt E (2015) Geomorph: Software for Geometric Morphometric Analyses. R package version 2.1.2. Available at https://CRAN.R-project.org/. Accessed April 30, 2016.
45. Adams DC, Otárola-Castillo E (2013) Geomorph: An R package for the collection and analysis of geometric morphometric shape data. *Methods Ecol Evol* 4:393–399.
46. Klingenberg CP (2011) MorphoJ: An integrated software package for geometric morphometrics. *Mol Ecol Resour* 11:353–357.
47. Arnold C, Matthews LJ, Nunn CL (2010) The 10kTrees website: A new online resource for primate phylogeny. *Evol Anthropol* 19:114–118.
48. Strait DS, Grine FE (2004) Inferring hominoid and early hominid phylogeny using craniodental characters: The role of fossil taxa. *J Hum Evol* 47:399–452.
49. Stevens NJ, et al. (2013) Palaeontological evidence for an Oligocene divergence between Old World monkeys and apes. *Nature* 497:611–614.
50. Gelman A, Rubin D (1992) Inferences from iterative simulation using multiple sequences. *Stat Sci* 7:457–511.
51. Khabbazian M, Kriebel R, Rohe K, Ané C (2016) Fast and accurate detection of evolutionary shifts in Ornstein–Uhlenbeck models. *Methods Ecol Evol* 7:811–824.
52. Cressler CE, Butler MA, King AA (2015) Detecting adaptive evolution in phylogenetic comparative analysis using the Ornstein–Uhlenbeck model. *Syst Biol* 64: 953–968.
53. Trinkaus E, Patel BA (2016) An early pleistocene human pedal phalanx from Swartkrans, SKX 16699, and the antiquity of the human lateral forefoot. *C R Palevol* 15:978–987.